

Wind induced pressure on 'Y' plan shape tall building

Sourav Mukherjee^{1a}, Souvik Chakraborty^{1b}, Sujit Kumar Dalui^{*2}
and Ashok Kumar Ahuja^{3c}

¹Bengal Engineering and Science University Shibpur, India

²Faculty of Engineering (Civil), Bengal Engineering and Science University, Shibpur, India

³Faculty of Engineering (Civil), Indian Institute of Technology Roorkee, India

(Received September 28, 2013, Revised July 11, 2014, Accepted August 31, 2014)

Abstract. This paper presents a comprehensive study of pressure developed on different faces of a 'Y' plan shape tall building using both numerical and experimental means. The experiment has been conducted in boundary layer wind tunnel located at Indian Institute of Technology Roorkee, India for flow condition corresponding to terrain category II of IS:875 (Part 3) – 1987, at a mean wind velocity of 10 m/s. Numerical study has been carried out under similar condition using computational fluid dynamics (CFD) package of ANSYS, namely ANSYS CFX. Two turbulence models, viz., k- ϵ and Shear Stress Transport (SST) have been used. Good conformity among the numerical and experimental results have been observed with SST model yielding results of higher magnitude. Peculiar pressure distribution on certain faces has been observed due to interference effect. Furthermore, flow pattern around the model has also been studied to explain the phenomenon occurring around the model.

Keywords: computational fluid dynamics (CFD); k- ϵ , shear stress transport (SST); interference effect; wind incidence angle; mean pressure coefficient

1. Introduction

In order to cope with the problem of increasing population and scarcity of land, all the major cities have stopped growing horizontally and started growing vertically. As a result, tall buildings are emerging all around the world. Naturally, wind load is critical for such structures. Fair amount of research have already been carried out on tall buildings. Davenport (1993) and Tse *et al.* (2009) have studied the effect of wind on rectangular plan buildings with the aid of wind tunnel experiment. Lin *et al.* (2004) discussed the findings of a wide spread wind-tunnel study on local wind forces on isolated tall buildings based on experimental outcome of nine square and rectangular models (1:500). The effects of elevation, aspect ratio and side ratio on the bluff body flow and on local wind forces were discussed. Blocken *et al.* (2005) carried out wind driven rain measurement on low rise building. The results obtained using computational fluid dynamics

*Corresponding author, Professor, E-mail: sujit_dalui@rediffmail.com

^a Post Graduate Student, Email: souravbecs.m@gmail.com

^b Post Graduate Student, Email: csouvik41@gmail.com

^c Professor, Email: ahuja_ak@rediffmail.com

package was compared with wind tunnel results. Huang *et al.* (2006) and Awruch (2009) investigated the wind effect on CAARC tall building with the help of CFD (Computational Fluid Dynamics) packages. Cluni *et al.* (2011), presented the effects of wind action on a regular building with a prismatic shape and an irregular tall buildings whose external shape was inspired by that of Bank of China Tower in Hong Kong with the help of higher order statistical moment analysis by the high frequency force balance (HFFB) technique. Some detailed field measurement of super tall buildings have also been conducted. Kim *et al.* (2008) conferred the effects of the taper ratio and the damping ratio on reducing the across-wind excitation of tall buildings by increasingly reduced velocity. The paper concluded that it is better to increase damping ratio than to increase tapering ratio to reduce the RMS across wind response. Fu *et al.* (2008) enumerated field measurements of the characteristics of boundary layer and storm response of two super tall buildings. The wind tunnel data showed good convergence with the field data. Au *et al.* (2012) carried out field investigation on modal properties of two tall buildings. Bashor *et al.* (2012) and Yi *et al.* (2013) have also performed field measurements of tall buildings. Other works carried out in the field of wind engineering include but are not limited to wind-induced natural ventilation (Cheng *et al.* 2011), wind resource assessment (Song *et al.* 2014), wind effect on bridges (Kwok *et al.* 2012) and reliability based design optimization of structures subjected to wind load (Spence and Gioffre 2012).

However, literature on irregular plan tall building is quite limited. Gomes *et al.* (2005) and Amin and Ahuja (2012) are among the few researchers to have investigated wind effect on irregular shapes. Further, insufficiency in information regarding irregular plans in various international wind load standards (ASCE 7-10, IS-875 (Part 3), AS/NZS: 1170.2, NBC (Part 4)) have called for research on this area.

In current work, wind generated pressure on different faces of a 'Y' plan shape tall building have been experimentally determined with help of wind tunnel tests. Further, the results have been compared with numerical results obtained from Computational Fluid Dynamics (CFD) package CFX. Although 'Y' plan is quite common, experimental data for such shape is quite rare. A brief study on such plan has been carried out by Hayashida and Iwasa (1990).

The objective of our current study is to assess the pressure generated on different faces of a 'Y' plan building due to different wind angles. Further, effect of change in wind incidence angle on pressure coefficient of different faces have also been studied.

2. Experimental program

2.1 Flow characteristics

The experiment was conducted at a boundary layer wind tunnel located at Indian Institute of Technology Roorkee, India. The wind tunnel is having a cross-sectional area of 2 m×2 m. The test section is 38 m long with a round table located at 12m from the upstream side (Fig. 1). Wind effects on the model for various wind incidence angle can be studied by rotating the round table at desired angle. The experimental flow was simulated similar to that of terrain category II as per Indian wind load code IS: 875 – 1987 (Part 3) at a geometric scale of 1:300. Terrain category II corresponds to open terrain with well scattered obstructions having height between 1.5 m to 10 m. Gradient height for terrain category II is 300m (1m in wind tunnel). The power law index (α) of the wind tunnel is 0.133. Mean wind speed of 10m/s was maintained in the wind tunnel. Blocks

and barrier walls were used to generate the boundary layer flow. Models were placed at a distance of 12 m from the upstream side. A reference pitot tube is located at a distance of 7.8 m to measure the free stream velocity in the test section. Hot wire anemometer, Manometer and Pressure transducers are also installed in the wind tunnel.

2.2 Details of model

The model used for testing (Fig. 2) was made of perspex sheet (having thickness 6 mm) at a geometric scale of 1:300. Fig. 3 shows a schematic diagram of the 'Y' plan shaped model. The dimension of smaller face of the 'Y' plan shaped model are 50 mm (length) × 500 mm (height) whereas that of larger faces are 100 mm (length) × 500 mm (height). While 27 pressure tapings were placed on the smaller face, 36 pressure tapings were placed on the larger one. The pressure on different faces were measured by rotating the model. The pressure tapings were placed as close as possible to the sidewalls and the top surface. To capture the high pressure (suction) zones occurring due to separation of flow, the pressure tapings are made of steel tube of 1 mm diameter and about 15-20 mm long. Pressure tapings are installed in the holes drilled in the form of a grid on all faces of building model.

2.3 Parametric study

The model was tested for wind incidence angle of 0° and 60°. Mean wind pressures on all the surfaces of the model were measured in order to study the pressure developed on such an irregular shape. Moreover, the effect of change in wind incidence angle has also been studied.

2.4 Measurement technique

First of all, velocity profile was measured at the test section i.e., at a distance of 12 m from upstream side (without building model) with a free stream velocity of 10 m/sec. For this purpose, a second pitot tube was used. Then 'Y' plan shaped building model was placed at a distance of 12 m (Fig. 1) from the upstream edge of the test section and wind pressure distribution on all surfaces of the building model was obtained using pressure transducer and data acquisition system. Modern data acquisitions system consisting of on-line processing of data by digital computers was used. The computer records the signals from Pressure transducers, analyze the signals and print or plot the results in desired form.

3. Numerical study

Numerical simulation has been carried out using Computational Fluid Dynamics (CFD) package of ANSYS, namely ANSYS CFX. Two models, viz. k- ϵ (Bardinal *et al.* 1997), Jones and Launder (1972), Launder and Sharma (1974)) and Shear Stress Transport (SST) (Menter 1994) have been used to simulate the turbulence. The modified continuity and momentum equation used for the numerical solution are given as:

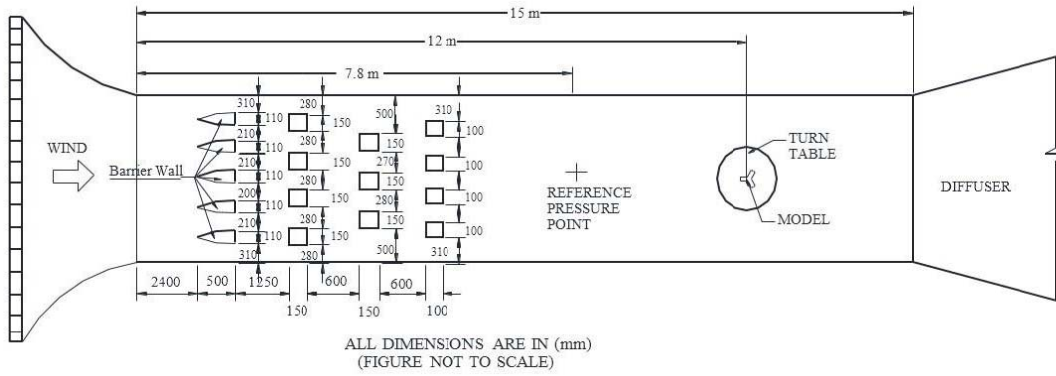


Fig. 1 Location of model in wind tunnel – plan view



Fig. 2 Y- shaped models in boundary layer wind tunnel

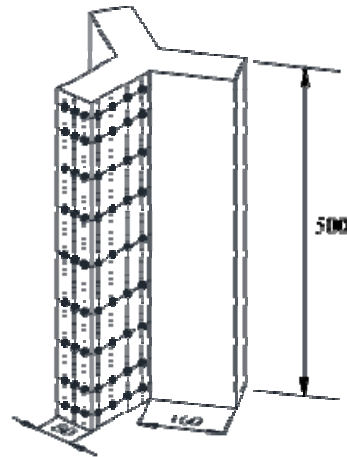


Fig. 3 Y- shaped models along with pressure tapping points

$$\frac{\partial \rho}{\partial t} + \frac{\partial \rho}{\partial x_j} (\rho U_j) = 0 \tag{1}$$

$$\frac{\partial \rho U_i}{\partial t} + \frac{\partial}{\partial x_j} (\rho U_i U_j) = -\frac{\partial P'}{\partial x_i} + \frac{\partial}{\partial x_j} [\mu_{eff} (\frac{\partial U_i}{\partial x_j} + \frac{\partial U_j}{\partial x_i})] + S_M \tag{2}$$

where S_M is the sum of body forces, μ_{eff} is the effective viscosity accounting for turbulence, and

P' is the modified pressure. ρ and U denote, respectively, density and velocity. The k- ε model is based on the eddy viscosity concept, so that

$$\mu_{\text{eff}} = \mu + \mu_t \quad (3)$$

μ_t is the turbulence viscosity. The k- ε model assumes that the turbulence viscosity is linked to the turbulence kinetic energy (k) and dissipation rate (ε) via the relation

$$\mu_t = C_\mu \rho \frac{k^2}{\varepsilon} \quad (4)$$

C_μ is a constant. The transport equations for k and ε are given as

$$\begin{aligned} \frac{\partial}{\partial t}(\rho k) + \frac{\partial}{\partial x_j}(\rho k u_j) &= \frac{\partial}{\partial x_j} \left[\left(\mu + \frac{\mu_t}{\sigma_k} \right) \frac{\partial k}{\partial x_j} \right] + G_k + G_b - \rho \varepsilon - Y_M + S_k \\ \frac{\partial}{\partial t}(\rho \varepsilon) + \frac{\partial}{\partial x_j}(\rho \varepsilon u_j) &= \frac{\partial}{\partial x_j} \left[\left(\mu + \frac{\mu_t}{\sigma_\varepsilon} \right) \frac{\partial \varepsilon}{\partial x_j} \right] + \rho C_1 S \varepsilon - \rho C_2 \frac{\varepsilon^2}{k + \sqrt{\nu \varepsilon}} + C_{1\varepsilon} \frac{\varepsilon}{k} C_{3\varepsilon} G_b + S_\varepsilon \end{aligned} \quad (5)$$

where

$$C_1 = \max\left[0.43, \frac{n}{n+5}\right], \quad n = S \frac{k}{\varepsilon}, \quad S = \sqrt{2S_{ij}S_{ij}} \quad (6)$$

G_k represents the generation of turbulence kinetic energy due to the mean velocity gradients, G_b is the generation of turbulence kinetic energy due to buoyancy and Y_m represents the contribution of the fluctuating dilatation in compressible turbulence to the overall dissipation rate, C_1 and C_2 are constants. σ_k and σ_ε are the turbulent Prandtl numbers for k (turbulence kinetic energy) and ε (dissipation rate). The values considered for $C_{2\varepsilon}$, σ_k and σ_ε are 1.9, 1 and 1.2 respectively.

A domain having 5H upwind fetch, 15H downwind fetch, 5H top clearance and 5H side clearance, where H is the height of the model, is considered (Franke *et al.* 2004) as shown in Fig. 4. Such a large size provides enough space for generation of vortex on the leeward side and avoids backflow of wind. Moreover no blockage correction is required. Tetrahedral elements are used for meshing the domain as well as the surface of the building (Fig. 5). The mesh size on vicinity of the model is comparatively smaller as compared to other location in order to accurately resolve the high gradient regions of fluid flow. Further, the mesh near the object boundaries has been inflated in order to avoid any unusual flow and have an accurate solid fluid interaction.

To obtain consistency between the numerical and experimental results, boundary condition (particularly inlet boundary condition) has to be defined identical to the experimental condition. Two kinds of expression, namely log law and power law are available to define atmospheric boundary layer (ABL) profile. The ABL profile in the boundary layer wind tunnel located at IIT Roorkee takes the following power law for terrain category II

$$\frac{U}{U_0} = \left(\frac{Y}{Y_0} \right)^\alpha \quad (7)$$

where U is the velocity at some particular height Y , U_0 is the boundary layer velocity, Y_0 is the

boundary layer depth and α is the exponent of the velocity profile and takes the value 0.133 in this case. The boundary layer velocity was considered as 10 m/s and reference pressure was considered as 1 atm. A comparison of ABL profile as obtained from wind tunnel and used for numerical analysis has been shown in Fig. 6. Further the variation of turbulence intensity with height has been shown in Fig. 7. The outlet has been modelled as a pressure outlet with relative pressure of 0 Pa. The side walls and the ground of the domain has been considered as free slip wall. However, the surface of the model are considered as no slip wall. The different boundary conditions are shown in Fig. 4.

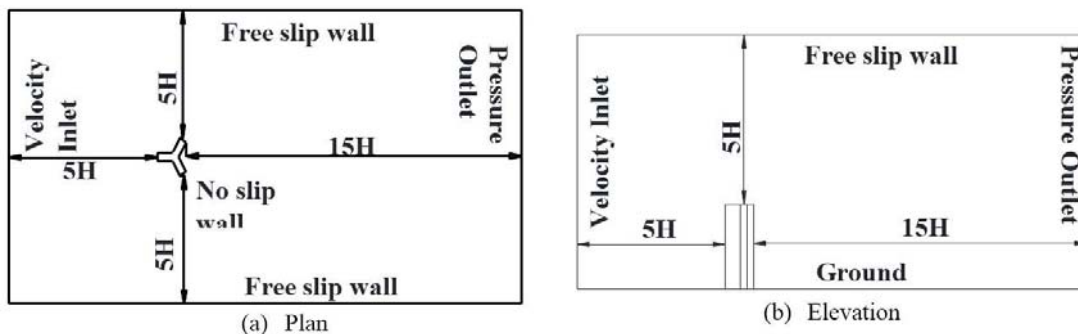


Fig. 4 Details of domain and boundary condition; (a) plan and (b) elevation

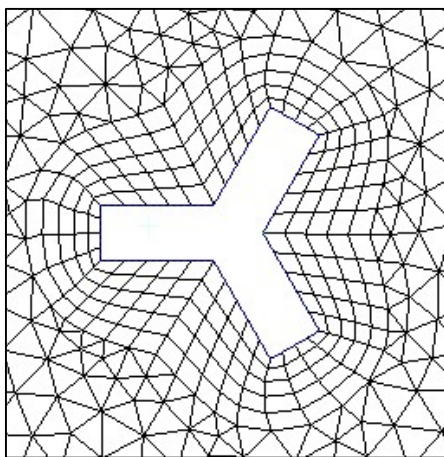


Fig. 5 Grid pattern around the model

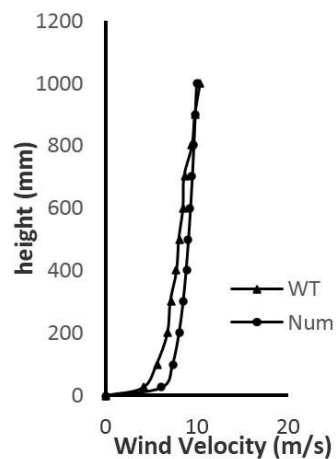


Fig. 6 Velocity profile near the model obtained from numerical and experimental method

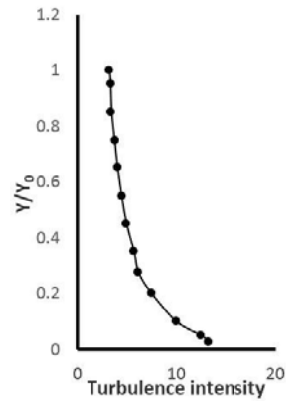


Fig. 7 Variation of turbulence intensity with height near the model

4. Results and discussion

4.1 Flow pattern

The flow pattern around the model for various wind angles, as obtained from k- ϵ method and SST method, are shown in Fig. 8 to Fig. 10. The wind sharply moves away from the edges of the windward side and reverts back after that. This results in high wind velocity at the corners of the windward side. Two symmetrical vortices have been formed in the wake region for wind incidence angle of 0° and 60°. Furthermore, the flow pattern for wind incidence angle of 0° and 60° are symmetric, resulting in identical pressure distribution on the symmetrical faces. For 90° wind angle, the vortices and the flow pattern are asymmetric in nature. As a consequence, all the faces are subjected to different pressure distribution.

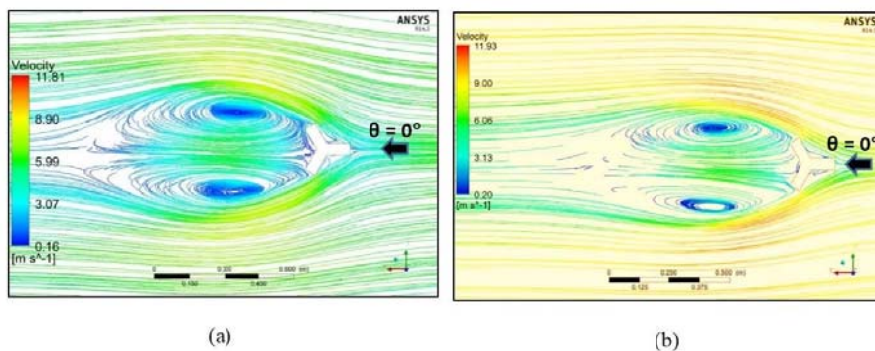


Fig. 8 Flow around the model for normal incidence angle; (a) k- ϵ method and (b) SST method

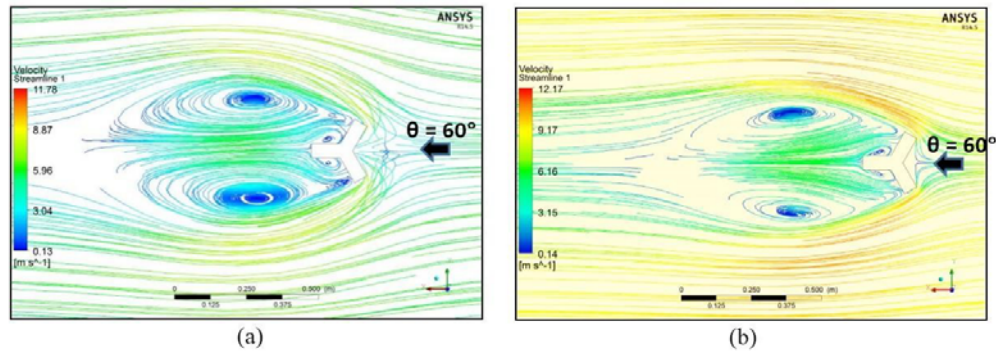


Fig. 9 Flow around the model for 60° wind angle; (a) k-ε method and (b) SST method

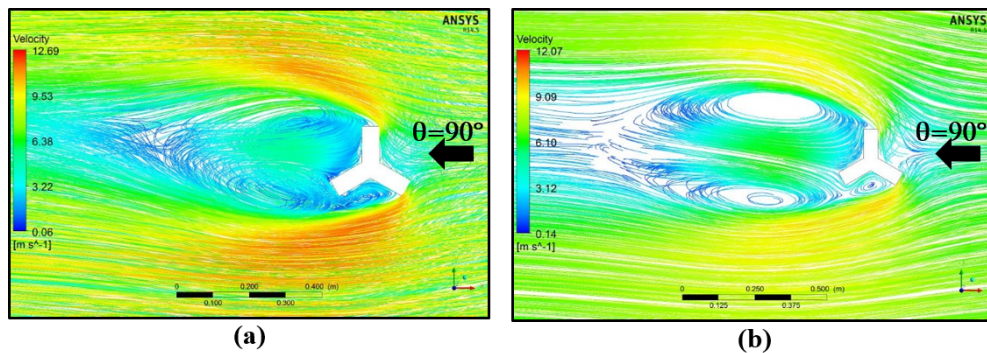


Fig. 10 Flow around the model for 90° wind angle; (a) k-ε method and (b) SST method

4.2 Pressure distribution

Nomenclature of different faces of the 'Y' plan shaped building is shown in Fig. 11. For 0° and 60° wind angles, the symmetrical faces are having identical pressure distribution due to symmetry in flow pattern and thus investigating pressure variation on five faces is sufficient to understand the pressure variation on all the faces of the 'Y' plan building. However for 90° wind incidence angle, investigating all the nine faces of the 'Y' plan shaped building is essential. Fig. 12 shows the pressure distribution on different faces of the model, as obtained from k-ε method, for normal incidence angle. As expected, positive pressure has been observed on Face A with maximum pressure at stagnation point. The pressure decreases as we move toward the edges. Furthermore, a symmetry in pressure variation is observed about the vertical centerline. Face B (B1 and B2) have experienced positive pressure due to interference effect of Face C (C1 and C2). Wind reverts back after hitting Face C and results in positive pressure on Face B. Face C is also subjected to positive pressure. However, the edge near Face D (D1 and D2) have experienced suction. Leeward faces, namely Face D and Face E (E1 and E2) are subjected to suction.

The pressure contours for 60° wind angle, as obtained from k-ε method are shown in Fig. 13. Face A and D2 are predominantly subjected to negative pressure with a thin line of high suction

near the edge due to separation of flow from the edges of Face B2. Face B2 and C2 are having identical pressure variation with maximum pressure at the stagnation zone. Leeward faces, viz., Face B1, C1, E2, E1 and D1 are subjected to suction. Pressure contour on Face D1 is symmetrical about the vertical centerline with maximum pressure near the top. Furthermore, Face B1 and C1 are having identical pressure distribution as that of Face E2 and E1 respectively.

The pressure contours for 90° wind angle, as obtained from k- ϵ method are shown in Fig. 14. While, faces B2, C2 and D2 are predominantly subjected to positive pressure, all the other faces have experienced suction. While maximum suction ($C_p = -1.22$) is observed on Face E2 due to separation of flow from the edge of Face D2, maximum positive pressure ($C_p = 1.00$) is observed on Face C2.

4.3 Experimental versus numerical results

Sectional plots showing the variation of pressure in terms of pressure coefficient at a height of 150 mm for wind incidence angle of 0° and 60° are shown in Figs. 15 and 16 respectively. Since no experiment was conducted for 90° wind angle, the sectional plot for the same has not been shown. The pressure distribution as obtained from the numerical models, namely k- ϵ and SST model, and the wind tunnel experiment are identical in nature. Even the pressure variation at the zones of separation of flow, i.e., Face B and face D is identical. However, SST method yields pressure coefficient of higher magnitude.

Figs. 17 and 18 shows the comparison of pressure coefficient along the vertical and horizontal centerline as obtained from the two numerical models and wind tunnel test for normal incidence angle. The results obtained from the two numerical method are having a good agreement with the experimental results with maximum discrepancy observed in case of Face D. For windward faces, the result obtained from k- ϵ model are having better agreement with the experimental results as observed from Fig. 16 whereas SST model yields better result for the leeward surfaces.

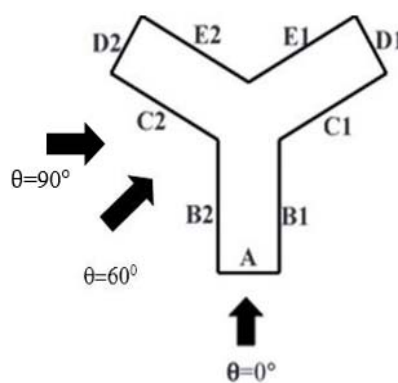


Fig. 11 Nomenclature of different faces of 'Y' plan model along with the two wind angles

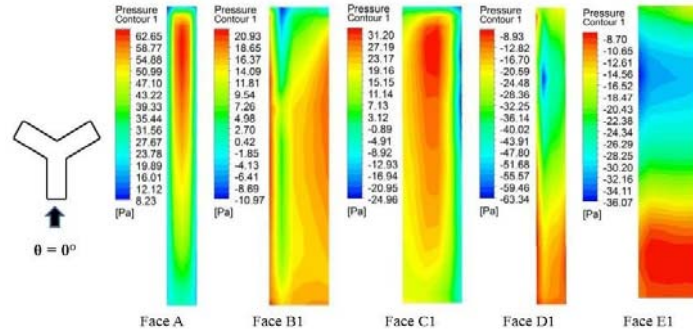


Fig. 12 Pressure contour on different face of 'Y' plan model for normal incidence angle

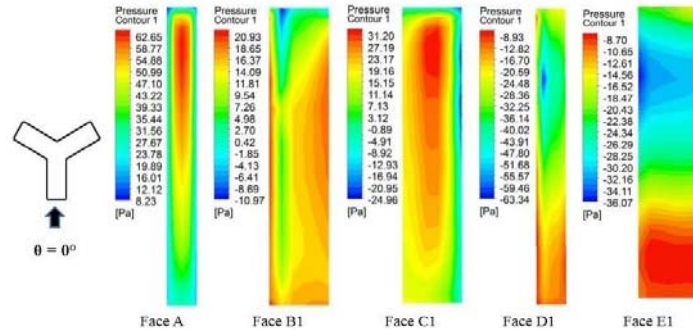


Fig. 13 Pressure contour on different face of 'Y' plan model for 60° wind angle

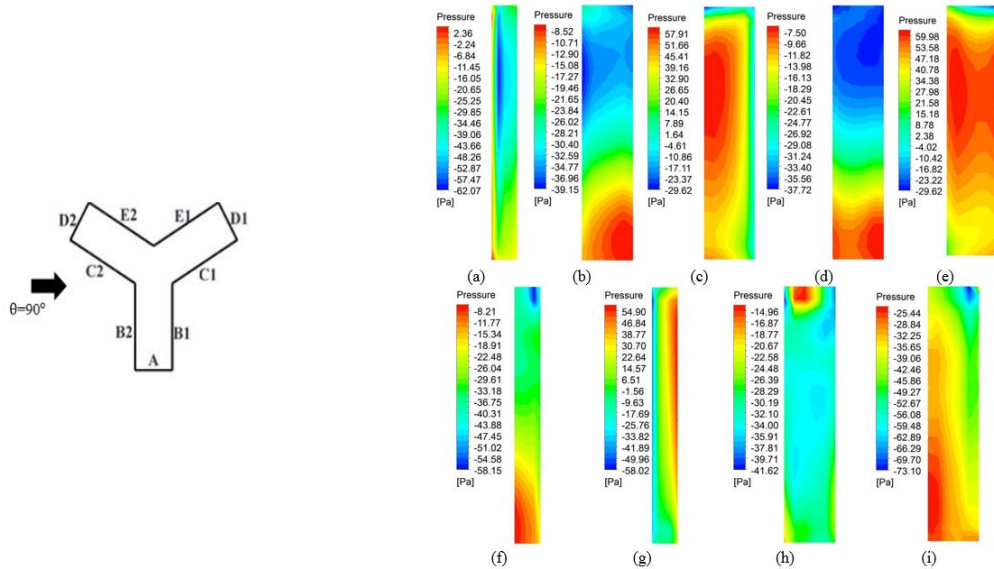


Fig. 14 Pressure contour on different face of 'Y' plan model for 90° wind angle; (a) Face A, (b) Face B1, (c) Face B2, (d) Face C1, (e) Face C2, (f) Face D1, (g) Face D2, (h) Face E1 and (i) Face E2

Figs. 19 and 20 demonstrates the pressure coefficient along the vertical and horizontal centerline as obtained from the two numerical models and wind tunnel test for 60° wind incidence angle. The general agreement among the results is quite good on all the surfaces. However on a closer inspection, SST model is found to overpredict the pressure generated on different faces of the model in low turbulent zone. As a result, pressure coefficient obtained from SST method on the top half of the building is having higher magnitude as compared to k-ε model and wind tunnel results. Similar to the normal incidence angle, k-ε model predicts accurate result along the horizontal centerline of the windward surfaces whereas SST model yields better result for the leeward surfaces.

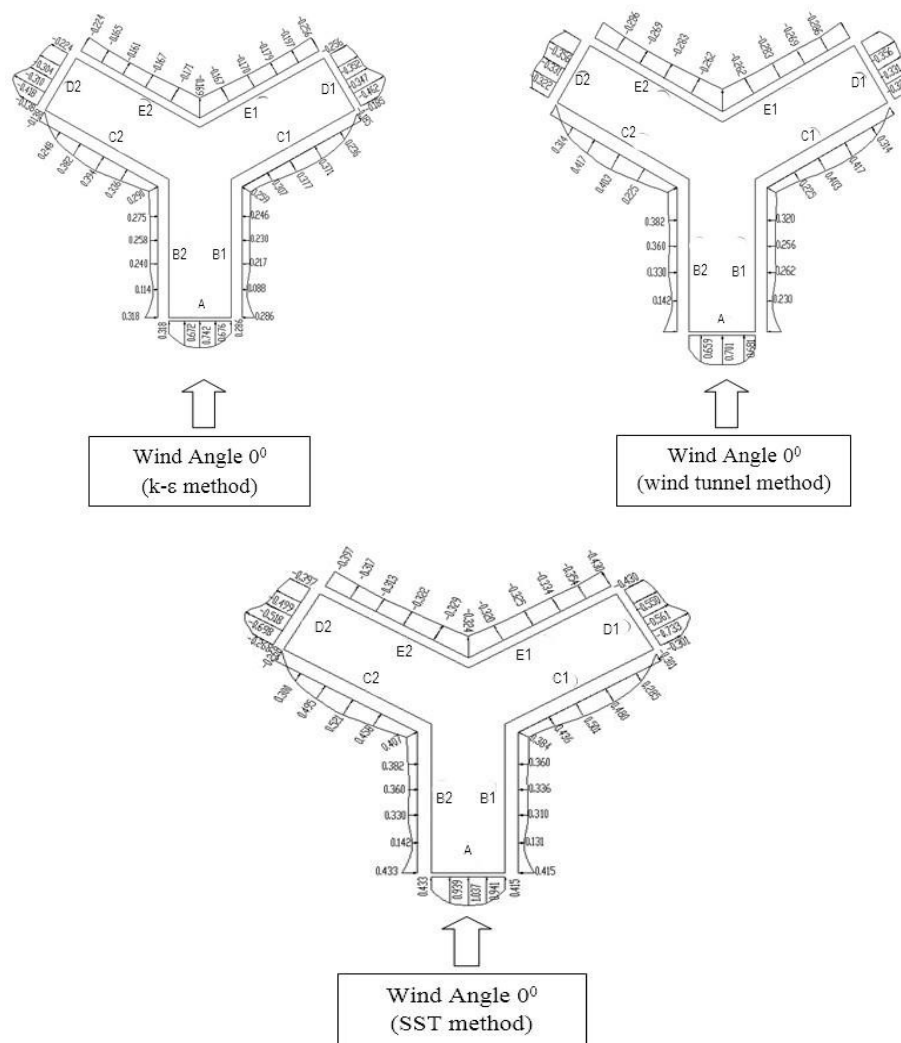


Fig. 15 Sectional plot of pressure at 0.15m height for 0° wind angle

Mean surface pressure coefficients on different faces of the ‘Y’ plan building as obtained from the experimental and numerical method have also been compared. While Table 1 presents the surface pressure coefficient for normal incidence angle, Table 2 presents the same for 60° wind angle. Good agreement among the experimental and the numerical methods has been observed with SST model yielding results of higher magnitude. SST model overpredicts the pressure at point of separation of flow. As a result, SST method have yielded quite high suction for Face D and Face E for normal incidence angle.

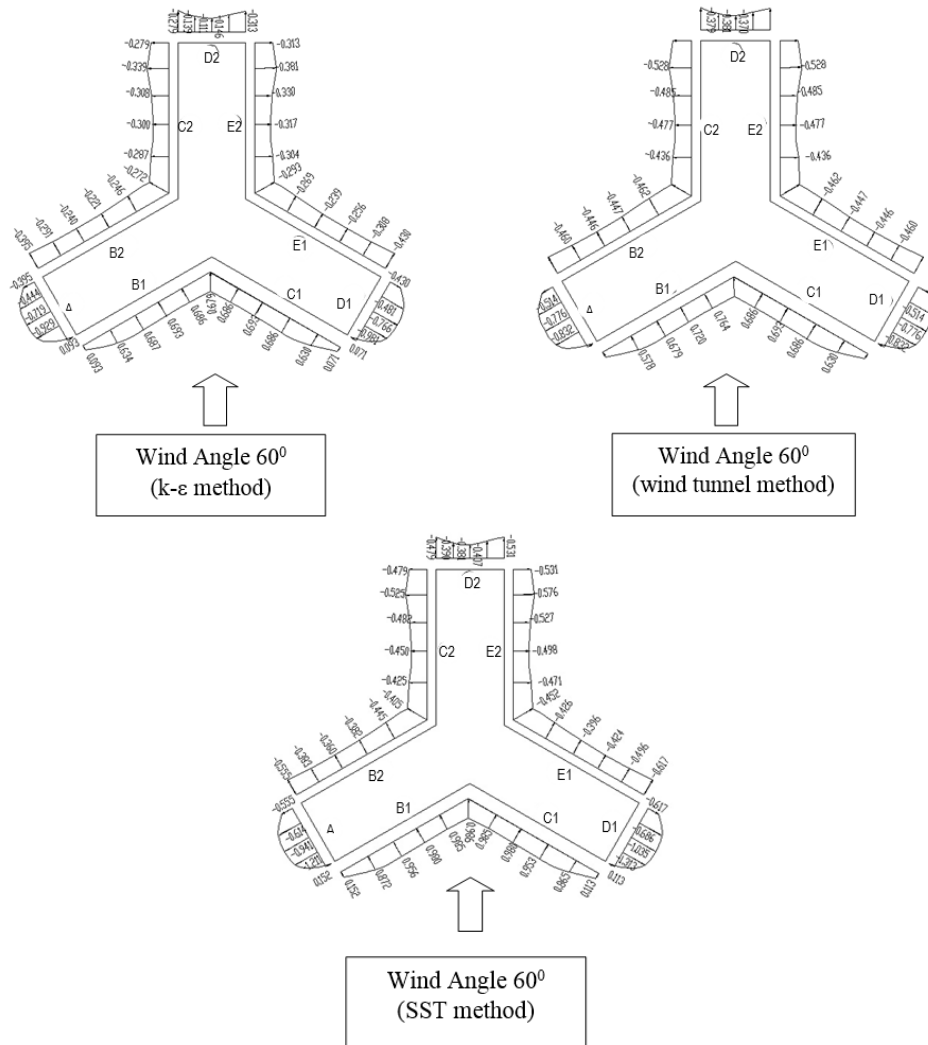


Fig. 16 Sectional plot of pressure at 0.15m height for 60° wind angle

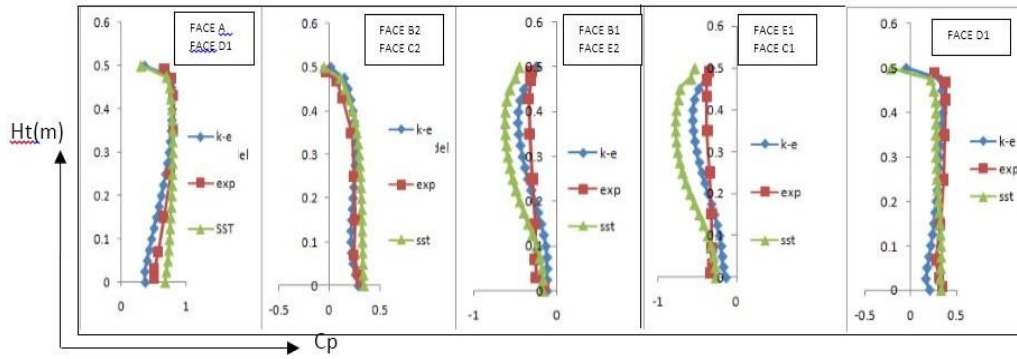


Fig. 17 Pressure co-efficient along the vertical centreline on different faces of 'Y' plan model for incidence angle 0°

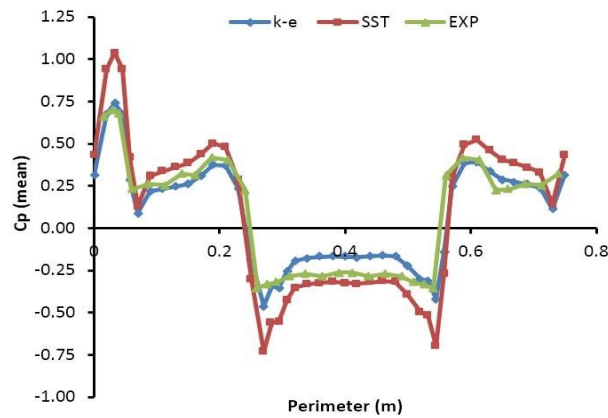


Fig. 18 Pressure coefficient along the horizontal centerline for normal incidence angle

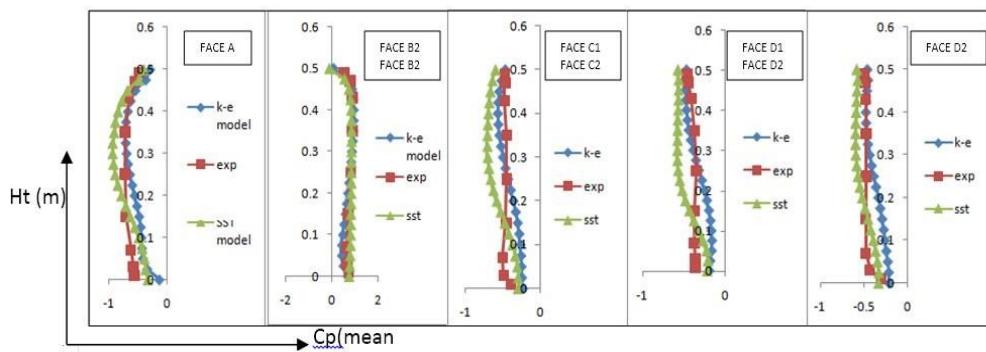


Fig. 19 Pressure co-efficient along the vertical centreline on different faces of 'Y' plan model for incidence angle 60°

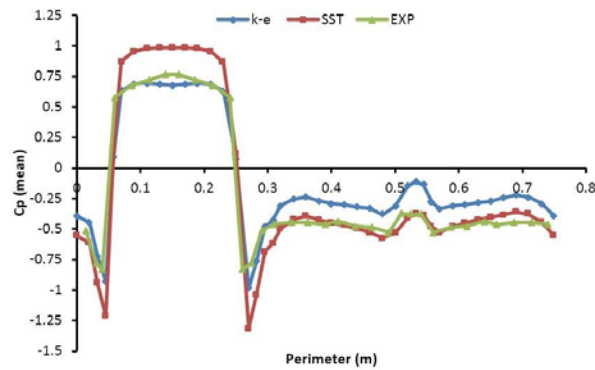


Fig. 20 Pressure coefficient along the horizontal centerline for 60° wind incidence angle

Table 1 Comparison of mean surface pressure coefficient on different faces of 'Y' plan building for normal incidence angle

Location	Mean C_p			Remarks
	k- ϵ	SST	Wind Tunnel	
FACE A	0.607	0.726	0.666	
FACE B1, FACE B2	0.224	0.267	0.189	
FACE C1, FACE C2	0.262	0.269	0.330	(-ve) indicates suction
FACE D1, FACE D2	-0.373	-0.572	-0.347	
FACE E1, FACE E2	-0.292	-0.442	-0.279	

Table 2 Comparison of mean surface pressure coefficient on different faces of 'Y' plan building for 60° wind incidence angle

Location	Mean C_p			Remarks
	k- ϵ	SST	Wind Tunnel	
FACE A, FACE D1	-0.523	-0.676	-0.621	
FACE B1, FACE C1	0.679	0.760	0.715	
FACE E1, FACE B2	-0.406	-0.551	-0.461	(-ve) indicates suction
FACE E2, FACE C2	-0.371	-0.512	-0.459	
FACE D2	-0.321	-0.475	-0.391	

4.4 Comparative study

Graphical plots representing effects of change of wind angle on different faces of the 'Y' plan building are shown in Figs. 21 and 22. Pressure on all the faces have been compared along the vertical centerline for the three wind incidence angles. The comparison along the perimeter has been carried out at a height of 0.35 m. The key features observed are discussed below:

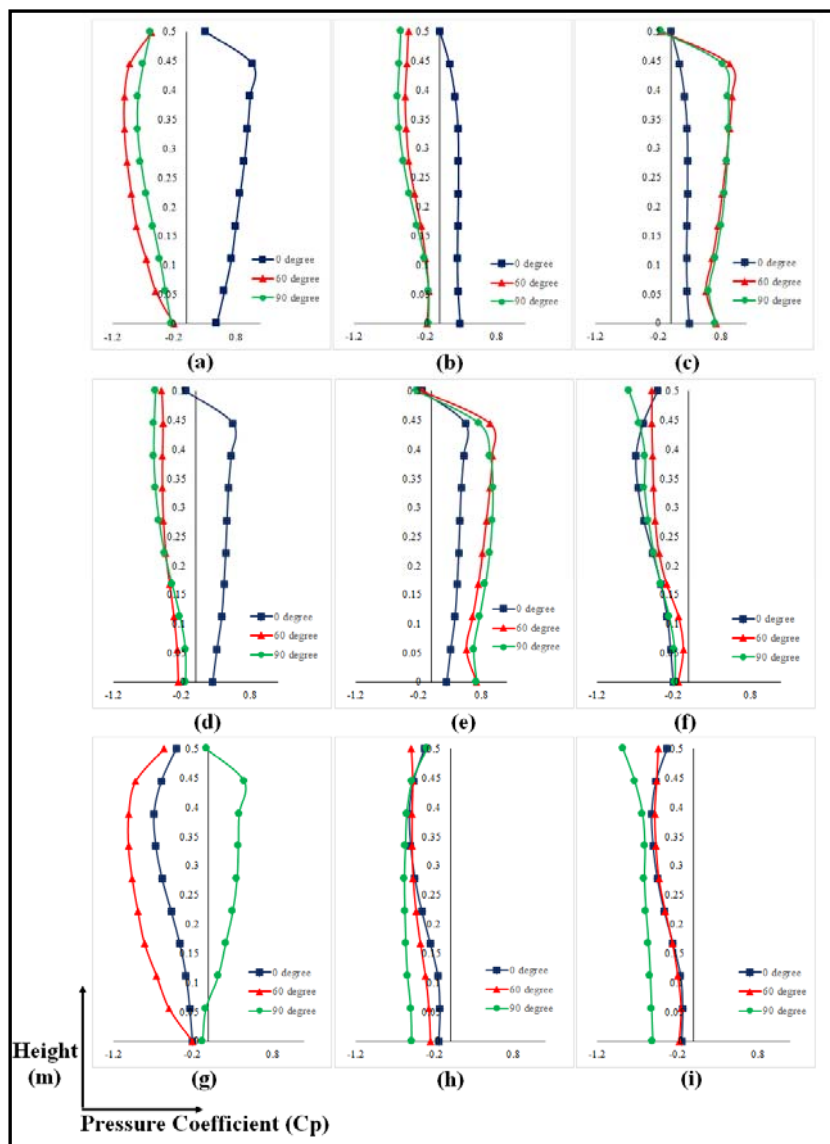


Fig. 21 Comparison of pressure coefficient along the vertical centerline on different faces of the 'Y' plan model; (a) Face A, (b) Face B1, (c) Face B2, (d) Face C1, (e) Face C2, (f) Face D1, (g) Face D2, (h) Face E1 and (i) Face E2

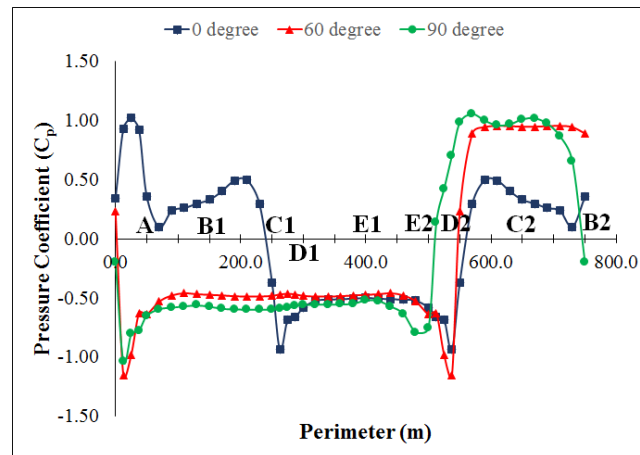


Fig. 22 Comparison of pressure coefficient along the perimeter of the 'Y' plan model at a height of 0.35m. The end point of each face is marked in the figure

- Nature of pressure on faces A, B1 and C1 has changed with change in wind angle (Figs. 20(a), 20(b) and 20(d)). While positive pressure is observed for normal incidence angle, suction is observed for 60° and 90° wind incidence angles.
- Face B2 and C2 have experienced positive pressure for all three wind incidence angles (Figs. 20(c) and 20(e)). Furthermore for Face B2 (Fig. 20(c)), pressure coefficient obtained for 60° and 90° wind angles are identical.
- Faces D1, E1 and E2 have experienced suction for all three wind incidence angles (Figs. 20(f), 20(h) and 20(i)). Furthermore for all the three faces, maximum suction is observed for 90° wind incidence angle.
- Although Face D2 has experience suction for 0° and 60° wind incidence angles, positive pressure is observed for 90° wind incidence angle (Fig. 20(g)).
- The nature of variation along the perimeter at 0.35m height for 60° and 90° wind angles are identical with only variation observed for Face D2 (Fig. 21).

5. Conclusions

Present study has shown that wind induced pressure on a 'Y' plan shape building is quite different from that of a regular rectangular plan building. The work was carried out with help of wind tunnel test and CFD simulation on this particular plan building for wind incidence angle of 0° and 60°. Two numerical models, namely k- ϵ and SST model has been used for the numerical simulation. The significant outcomes of the current study are summarized as follow:

1. Symmetry in flow pattern has resulted in identical pressure distribution on symmetrical faces for 0° and 60°, 90° wind angles. However, no such symmetry is present for 90° wind angle.

2. For normal incidence angle, side faces, namely Face B1 and B2 have experienced positive pressure due to interference effect. However no such interference effect is observed for 60° and 90° wind angle.
3. Good agreement has been observed among the numerical and experimental results. Overall accuracy of k-ε model is better as compared to SST model. However, SST model predicts pressure in high turbulence zone with higher degree of accuracy.
4. Nature of pressure on Face A, B1 and C1 has reversed due to change in wind angle. While positive pressure is observed for 0° wind angle, suction occurs for 60° and 90° wind angles.
5. Critical pressure on faces B1, D1, E1 and E2 is observed for 90° wind angle. Similarly, faces B2, C2 and D2 have experienced critical pressure for 60° wind angle.

Acknowledgements

Authors would like to express their sincere gratitude to Department of Science and Technology (DST), New Delhi, India for providing funding to conduct the experiment. The authors would also like to express their gratitude to the anonymous reviewers for their detailed and useful comments to the manuscript.

References

- Amin, J.A. and Ahuja, A.K. (2012), "Wind-induced mean interference effects between two Closed spaced buildings", *KSCCE*, **16**(1), 119-131.
- ANSYS (2012), Inc., Tutorial for ANSYS CFX 14.5, 2012.
- AS/NZS: 1170.2 (2002), *Structural Design Actions, Part 2: Wind Actions*, Standards Australia/Standards New Zealand, Sydney, Wellington.
- ASCE: 7-10 (2010), *Minimum Design Loads for Buildings and Other Structures*, Structural Engineering Institute of the American Society of Civil Engineering, Reston.
- Au, S.K., Zhang, F.L. and To, P. (2012), "Field observations on modal properties of two tall buildings under strong wind", *J. Wind Eng. Ind. Aerod.*, **101**, 12-23.
- Bardina, J.E., Huang, P.G. and Coakley, T.J. (1997), *Turbulence Modeling Validation, Testing, and Development*, NASA Technical Memorandum 110446.
- Bashor, R., Bobby, S., Kijewski-Correa, T. and Kareem, A. (2012), "Full-scale performance evaluation of tall buildings under wind", *J. Wind Eng. Ind. Aerod.*, **104-106**, 88-97.
- Blocken, B. and Carmeliet, J. (2005), "High resolution wind-driven rain measurements on a low-rise building-experimental data for model development and model validation", *J. Wind Eng. Ind. Aerod.*, **93**(12), 905-928
- Braun, A.L. and Awruch, A.M. (2009), "Aerodynamic and aeroelastic analyses on the CAARC standard tall building model using numerical simulation", *J. Wind Eng. Ind. Aerod.*, **87**(9-10), 564-581.
- Cheng, C.K.C., Lam, K.M., Leung, Y.T.A., Yang, K., Li Danny, H.W. and Cheung Sherman, C.P. (2011), "Wind-induced natural ventilation of re-entrant bays in a high-rise building", *J. Wind Eng. Ind. Aerod.*, **99**(2-3), 79-90.
- Cluni, F., Gusella, V., Spence, S.M.J. and Bartoli, G. (2011), "Wind action on regular and irregular tall buildings: Higher order moment statistical analysis by HFFB and SMPSS measurements", *J. Wind Eng. Ind. Aerod.*, **99**(6-7), 682-690.
- Davenport, A.G. (1993), *The response of slender structures to wind*, Wind Climate in Cities, (Ed., Cermak *et al.*), Germany.

- Franke, J., Hirsch, C., Jensen, A., Krüs, H., Schatzmann, M., Westbury, P., Miles, S., Wisse, J. and Wright, N.G. (2004), Recommendations on the use of CFD in Wind Engineering, COST Action C14: Impact of Wind and Storm on City Life and Built Environment, von Karman Institute for Fluid Dynamics.
- Fu, J.Y., Li, Q.S., Wu, J.R., Xiao, Y.Q. and Song, L.L.(2008), “Field measurement of boundary layer wind characteristics and wind induced response of super tall buildings”, *J. Wind Eng. Ind. Aerod.*, **96**(8-9), 1332-1358.
- Gomes, M., Rodrigues, A. and Mendes, P. (2005), “Experimental and numerical study of wind pressure on irregular-plan shapes”, *J. Wind Eng. Ind. Aerod.*, **93**(10), 741-756.
- Hayashida, H. and Iwasa, Y. (1990) “Aerodynamic shape effects of tall buildings for vortex induced vibration”, *J. Wind Eng. Ind. Aerod.*, **33** (1-2), 237-242.
- IS: 875 (1987), “Indian Standard Code of Practice for Design Loads (Other than Earthquake) For Buildings And Structures, Part 3 (Wind Loads)” Bureau Of Indian Standards, New Delhi.
- Jones, W.P. and Launder, B.E. (1972), “The prediction of laminarization with a two-equation model of turbulence”, *Int. J. Heat Mass Trans.*, **15**, 301-314.
- Kim, Y., You, K. and Ko, N. (2008), “Across-wind responses of an aeroelastic tapered tall building”, *J. Wind Eng. Ind. Aerod.*, **96**(8-9), 1307-1319.
- Kwok, K.C.S., Qin, X.R., Fok, C.H. and Hitchcock, P.A. (2011), “Wind-induced pressures around a sectional twin-deck bridge model: effects of gap-width on the aerodynamic forces and vortex shedding mechanisms”, *J. Wind Eng. Ind. Aerod.*, **110**, 50-61.
- Launder, B.E. and Sharma, B.I. (1974), “Application of the energy dissipation model of turbulence to the calculation of flow near a spinning disc”, *Lett. Heat Mass. Transfer*, **1**(2), 131-138.
- Lin, N., Letchford, C., Tamura, Y. and Liang, B. (2004), “Characteristics of wind forces acting on tall buildings”, *J. Wind Eng. Ind. Aerod.*, **93**(3), 217-242.
- Menter, F.R. (1994), “Two-equation eddy-viscosity turbulence models for engineering applications”, *AIAA J.*, **32**(8), 1598-1605
- NBC (Part-4) (1995), *Structural commentaries*, National Research Council of Canada.
- Simiu, E. and Scanlan, R.H. (1996), *Wind Effects on Structures*, 2nd Ed., John Wiley & Sons, New York.
- Spence, M.J.S. and Gioffrè, M. (2012), “Large scale reliability-based design optimization of wind excited tall buildings”, *Probabilist Eng. Mech.*, **28**, 206-215.
- Song, M.X., Chen, K., He, Z.Y. and Zhang, X. (2014) “Wind resource assessment on complex terrain based on observations of a single anemometer”, *J. Wind Eng. Ind. Aerod.*, **125**, 22-29
- Stathopoulos, T. and Baniotopoulos, C.C. (2007), *Wind Effects on Buildings and Design of Wind-Sensitive Structures*, Springer Wien New York, Udine, Italy.
- Tse, K.T., Hitchcock, P.A., Kwok, K.C.S. and Chan, C.M. (2009), “Economic perspectives of aerodynamic treatments of square tall buildings”, *J. Wind Eng. Ind. Aerod.*, **97**(9-10), 455 -467.
- Tu, J., Yeoh, G.H. and Liu, C. (2008), *Computational Fluid Dynamics A practical Approach*, Elsevier, New Delhi, India.
- Yi, J., Zhang, J.W. and Li, Q.S. (2013), “Dynamic characteristics and wind-induced responses of a super-tall building during typhoons”, *J. Wind Eng. Ind. Aerod.*, **121**, 116-130.